Food Bioprocess Technol (2014) 7:1160–1170
DOI 10.1007/s11947-013-1162-0

ORIGINAL PAPER

Micropores and Their Relationship with Carotenoids Stability: A New Tool to Study Preservation of Solid Foods

Luz A. Pascual-Pineda · Enrique Flores-Andrade · Liliana Alamilla-Beltrán · Jose J. Chanona-Pérez · César I. Beristain · Gustavo F. Gutiérrez-López · Ebner Azuara

Received: 19 January 2013 / Accepted: 12 July 2013 / Published online: 31 July 2013

Abstract Carotenoids were encapsulated by means of coacervation by using a nanostructured material (NE) prepared with alginate/zeolite valfor 100 (1:3) and another that was non-nanostructured (AA) prepared with alginate at 2 %. The diameter of the AA and NE capsules was ≈1,200 μm. The NE protected the carotenoids at higher water activities (a_w) than the AA. The highest retention of carotenoids (7,200 mg/kg dry solids for NE and 2,230 mg/kg dry solids for AA) was observed at water activities corresponding to the minimal integral entropy (≈0.35–0.45 for NE and ≈0.1 for AA). According to the enthalpy–entropy compensation, the water adsorption in the AA capsules was enthalpy driven at a_w range of 0.115–0.973. However, the NE showed two zones: (1) at low a_w (0.115–0.4), the water adsorption was controlled by entropy and (2) over an a_w range of 0.4–0.973, controlled by enthalpy. Atomic force microscope images, moisture content corresponding to micropore volume and thermodynamic properties suggest that the adsorption process and the carotenoids stability were controlled by entropic barriers when the water molecules were adsorbed in the micropores (nanopores with pore diameter <2 nm). The practical use of these results is that increasing the number of micropores in the solid matrix of wall materials is possible to improve the preservation of nutrients and functional substances during processing and storage of foods.

Keywords Carotenoids stability · Nanotechnology · Thermodynamic properties

Nomenclature

AA	Capsules of ammonium–calcium alginate
A_{472}	Absorption at 472 nm
A_{508}	Absorption at 508 nm
a_w	Water activity
a*	Color parameter (red)
b*	Color parameter (yellow)
B	Constant related to the microporous structure of the adsorbent
C	Maximum water adsorption by weakly binding sites (in gram water per 100 g dry solids) in Equation (1)
C^R	Red isochromic carotenoid pigment content (in milligram per kilogram dry solids)
C^Y	Yellow isochromic carotenoid pigment content (in milligram per kilogram dry solids)
C^T	Total carotenoid content
D	Constant of adsorption in Eq. (5)
H_V (T)	Integral molar heat of adsorption of water (in joule per mole)

L. A. Pascual-Pineda
Dirección General de Investigaciones, Universidad Veracruzana, Av. Luis Castelazo Ayala s/n. Colonia Industrial Ánimas, C. P. 91190 Xalapa, Veracruz, Mexico

E. Flores-Andrade
Facultad de Ciencias Químicas de la Universidad Veracruzana, Prolongación Oriente 6, Orizaba, Veracruz C. P. 94340, Mexico

L. Alamilla-Beltrán · J. J. Chanona-Pérez · G. F. Gutiérrez-López
Escuela Nacional de Ciencias Biológicas del Instituto Politécnico Nacional, Prolongación de Carpio y Plan de Ayala, Colonia Plutarco Elías Calles, Delegación Miguel Hidalgo, Código Postal 11340 México City, Distrito Federal, Mexico

C. I. Beristain · E. Azuara (✉)
Instituto de Ciencias Básicas de la Universidad Veracruzana, Calle Dr. Rafael Sánchez Altamirano S/N, Colonia Industrial Animas, Xalapa, Veracruz Código Postal 91192, Mexico
e-mail: eazuara@uv.mx

$H_v^0(T)$	Heat of condensation of pure water (in joule per mole)
$K_a^{'}$	Maximum water adsorption by strongly binding sites (in gram water per 100 g dry solids) in Equation 1
K_a	A dimensional measure of attraction of the primary sites for the adsorbate
$K_b^{'}$	Maximum water adsorption at secondary sites (in gram water per 100 g dry solids) in Equation 1
k_b	A dimensional measure of attraction of the secondary sites for the adsorbate
M	Equilibrium moisture content
m	Number of data pairs $[(\Delta H_{int})_T, (\Delta S_{int})_T]$
Mc_i	Calculated moisture content
Me_i	Experimental moisture content
N	Number of experimental data
n	Number of isotherms used
N_1	Moles of adsorbed water
NE	Capsules with ZV and ammonium–calcium alginate
P	Mean relative deviation modulus (in percent)
P_v	Partial pressure of water in a food (in newton per square meter)
P_v^0	Vapour pressure of water at the same temperature (in newton per square meter)
R	Universal gas constant (in joule per mole kelvin)
S	Total entropy of adsorbed water molecules (in joule per mole kelvin)
S_L	Molar entropy of pure liquid water in equilibrium with vapour (in joule per mole kelvin)
$S_s=S/N_1$	Integral entropy of water adsorbed in the adsorbent (in joule per mole kelvin)
T	Sorption isotherm temperature (in kelvin)
T_B	Isokinetic temperature (in kelvin)
T_{hm}	Harmonic mean temperature (in kelvin)
V_{TB}	Standard error of the isokinetic temperature
W_{ap}	Molecular weight of the adsorbent
W_v	Molecular weight of the water
X	Moisture content (in gram of water per 100 g dry solids)
X_0	Moisture content corresponding to the micropore volume (in gram of water per 100 g dry solids)
ZV	Zeolite valfor 100
φ	Surface potential (in joule per square meter)
ΔG	Change in Gibbs free energy (in joule per mole)
ΔG_B	Change in Gibbs free energy at isokinetic temperature (in joule per mole)
ΔH_{int}	Change in enthalpy (in joule per mole)
$\overline{\Delta H}_{int}$	Average enthalpy
ΔS_{int}	Change in entropy (in joule per mole kelvin)
$\overline{\Delta S}_{int}$	Average entropy
μ_a	Chemical potential of the adsorbent participating in the condensed phase (in joule per mole)
μ_{ap}	Chemical potential of the pure adsorbent (in joule per mole)

Introduction

The behaviour of water confined in nanoscale spaces differs from that of water at the macroscopic level. According to IUPAC (1985), pores are classified into the three groups: (1) macropores, having diameters larger than 50 nm, (2) mesopores, with diameters between 2 and 50 nm and (3) micropores, which diameters are smaller than 2 nm. Iiyama et al. (1997) demonstrated by X-ray diffraction that the adsorbed water molecules in hydrophobic micropores of activated carbon fibres had a more orderly structure, similar to the structure of ice. Using computer simulations, Hummer et al. (2001) studied the conduction of water through the hydrophobic channels of carbon nanotubes 13.5 Å long and 8 Å in diameter, where the water continuously and spontaneously filled the inside of a nonpolar structure; once inside, the water became ordered in a row of five water molecules. These discoveries have shown the importance of studying the physicochemical nature of water in solid foods to understand its effect on food stability.

The moisture sorption isotherm is a relationship between water activity and moisture content at a given temperature. It is useful in the analysis of processes affecting the physical, biochemical, and microbiological stability of foods (Tsami et al. 1990). The adsorption isotherms are useful to obtain information about the physicochemical binding of water during storage of dried foods (Hill and Rizvi 1982).

Thermodynamic functions are readily calculated from sorption isotherms, thus facilitating a thorough interpretation of the isotherm process and providing further insight into the sorption mechanisms (Rizvi and Benado 1984). Enthalpy change (ΔH) provides a measure of the energy variations occurring on mixing water molecules with sorbent during sorption processes. Entropy (ΔS) may be related with the binding or repulsive forces in the system and is associated with the spatial arrangements at the water-sorbent interface (McMinn et al. 2005). The minimum integral entropy has been proposed as the most appropriate indicator for determining the best storage conditions (Beristain and Azuara 1990; Domínguez et al. 2007). However, there has been little research into the nanoporous structure and its relation to the minimum integral entropy (Azuara and Beristain 2006; Azuara and Beristain 2007).

A linear relationship between the entropy and enthalpy change has been observed in a variety of processes (Chodera and Mobley 2013; Rudra et al. 2008). Labuza (1980) described applications of the enthalpy–entropy compensation law to reactions related to foods, and Beristain et al. (1996) demonstrated that the enthalpy–entropy compensation is a useful tool for obtaining information regarding the mechanisms that control

water vapour sorption in foods. Azuara and Beristain (2006) proposed that while water adsorption occurs in the micropores, the adsorption process is controlled by entropy.

Alginate is the principal biomacromolecule extracted from brown seaweeds and consists of linear chains of α-L-guluronic acid (G) and β-D-mannuronic acid (M) residues joined by 1,4 glycosidic linkages forming regions of M-blocks, G-blocks and blocks of alternating sequence (MG-blocks), where the relative proportions of these sequential organizations depends on the source (Johnson et al. 1997). Soluble sodium alginate can be crosslinked using calcium chloride with formation of insoluble calcium alginate particles in the size range of 100 nm to 2 mm (Babu et al. 2007; Martins et al. 2007). As hydrophilic polymer, alginate has a tendency to adsorb water from the surrounding environment, showing a typical behaviour of type III isotherms, according to Brunauer et al. (1940), this feature is indicative of weak adsorbent–adsorbate interactions (Rouquerol et al. 1999).

Almost all of the zeolites (especially high Al containing) show type I water sorption isotherm, which indicate the high affinity to water at low partial pressure (Ng and Mintova 2008). The exploitation of these properties underlies the use of zeolites in a wide range of industrial and agricultural applications (Papaioannou et al. 2005).

Paprika (powder, flakes, or oleoresin) is obtained from the ripe fruit of *Capsicum annuum* L., which is a spice widely used for culinary and industrial purposes, such as food coloring and, in some cases, for its peculiar pungency (Topuz et al. 2009; Topuz 2008). During its processing and storage, paprika is susceptible to discoloration due to the degradation of carotenoids and non-enzymatic browning reactions (Topuz 2008). The objective of this work was four-fold: (1) to encapsulate paprika oleoresin by means of coacervation to produce two model food systems, one with a nanostructured material (NE) prepared with (alginate+zeolite valfor) and another with a non-nanostructured material (AA) prepared with alginate; (2) to evaluate the adsorption process of the capsules AA and NE using integral thermodynamic properties, (3) to study in the two model food systems (AA and NE) the effect of wall material nanocavities on the stability of carotenoids and predict the adequate storage conditions (water activity and temperature) by calculating the minimum integral entropy of the water vapour molecules adsorbed on the surface of the capsules AA and NE, and (4) to determine the enthalpic and entropic mechanisms of water vapour adsorption on the capsules of paprika oleoresin.

Materials and Methods

Materials

Alginic acid (ammonium salt) extracted from *Macrocystis pyrifera* which holds 20 % of the G blocks was purchased from Sigma Chemical Co. (St. Louis, Mo., USA). Zeolite valfor 100 of 0.4 nm of pore diameter was donated by Silicatos y Derivados de México, Mexico City. Anhydrous calcium chloride was purchased from Fisher Scientific Co. (Fair Lawn, N.J., USA). Paprika oleoresin 100,000 units, 46 % of red pigment and 54 % of yellow pigments was obtained from AMCO (Mexico City).

Preparation of Nanostructured (NE) and Non-nanostructured (AA) Capsules

Two aqueous solutions of ammonium–calcium alginate of *M. pyrifera* were prepared as follows: (1) Aqueous solution A with 8 % (*w*/*v*) total solids and a 1:3, alginate/zeolite valfor 100 ratio used to produce nanostructured capsules (NE), and (2) A 2 % alginate aqueous solution B used to produce non-nanostructured capsules (AA). Subsequently, paprika oleoresin was added to both aqueous solutions at a ratio of 1:0.5 (solids/oleoresin). The capsules were produced by dripping solutions A and B containing the paprika essential oil to a 2 % $CaCl_2$ aqueous solution. Finally, the capsules were lyophilized by using a freeze dryer (Labconco Model Look Lyph 4.5, USA) during 24 h.

Moisture Sorption Isotherms

The adsorption of water vapour in the capsules was determined by the gravimetric method (Lang et al. 1981). To achieve almost zero moisture, the capsules were placed in vacuum desiccators containing P_2O_5 for a week, and the zeolite valfor 100 (ZV) was dried in an oven at 600 °C during 4 h. Later on, 1–2 g samples were placed in triplicate in desiccators with saturated salts in a range from 0.11 to 0.97 water activity. The samples were stored at 15, 25, and 35 °C to achieve equilibrium.

Modeling of Moisture Sorption Isotherms

The D'Arcy and Watt (DW) equation was used in modeling water sorption (D'Arcy and Watt 1970):

$$M = \frac{K_a' k_a a_w}{1 + k_a a_w} + \frac{K_b' k_b a_w}{1 - k_b a_w} + Ca_w \quad (1)$$

This model is represented by a composite curve of three isotherms arising from three different processes and in which: K'_a is the maximum water adsorption by strongly binding sites, K'_b is the maximum water adsorption at secondary sites and C is the maximum water adsorption by weakly binding sites.

Goodness of fit was evaluated using the average of the relative percentage difference between the experimental and

predicted values of the moisture content or mean relative deviation modulus (P), defined by the following equation (Lomauro et al. 1985):

$$P(\%) = \frac{100}{N}\sum_{i=1}^{N}\frac{|\mathrm{Me}_i - \mathrm{Mc}_i|}{\mathrm{Me}_i} \quad (2)$$

Determination of the Enthalpy and Entropy of Sorption

The integral enthalpies and entropies of sorption were calculated from the adsorption isotherms by using the method reported by Azuara and Beristain (2006). The Gibbs free energy (ΔG) was calculated with the following equation:

$$\Delta G = RT \ln a_w \quad (3)$$

The integral enthalpy changes in the interface at different stages of the adsorption process were determined with Othmer's equation (Othmer 1940):

$$\frac{\mathrm{d}\ln P_V}{\mathrm{d}\ln P_v^0} = \frac{H_V(T)}{H_v^0(T)} \quad (4)$$

Since all these terms are temperature dependent, the equation can be integrated:

$$\ln P_V = \left[\frac{H_V(T)}{H_V^0(T)}\right]_\varphi \ln P_V^0 + D \quad (5)$$

The integral molar enthalpy (ΔH_{int}) at a constant surface potential is given by

$$(\Delta H_{\mathrm{int}})_T = \left[\frac{H_V(T)}{H_V^0(T)} - 1\right]_\varphi H_v^0(T) \quad (6)$$

$$\varphi = \mu_{ap} - \mu_a = RT\frac{W_{ap}}{W_v}\int_0^{a_w} M d\ln a_w \quad (7)$$

By calculating $(H_V T)/H_v^0(T)$ from Equation (5) and substituting it into Eq. (7), it becomes possible to calculate the integral enthalpy at different temperatures, provided that a good means of estimating $H_v^0(T)$ is available, such as that proposed by Wexler (1976):

$$H_v^0(T) = 6.15\times 10^4 - 94.14T + 17.74\times 10^{-2}T^2 - 2.03\times 10^{-4}T^3 \quad (8)$$

Using the values obtained for (ΔH_{int}) changes, the molar integral entropy (ΔS_{int}) can be estimated using the following equation:

$$(\Delta S_{\mathrm{int}})_T = S_S - S_L = -\frac{(\Delta H_{\mathrm{int}})_T}{T} - R\ln a_w \quad (9)$$

Compensation Theory

The entropic and enthalpic mechanisms that dominated in the process of water adsorption were determined by relating the integral enthalpy $(\Delta H_{\mathrm{int}})_T$ and integral entropy $(\Delta S_{\mathrm{int}})_T$ with the law of compensation (Beristain et al. 1996):

$$(\Delta H_{\mathrm{int}})_T = T_B(\Delta S_{\mathrm{int}}) + \Delta G_B \quad (10)$$

All the calculated regression coefficients are acceptable; however, in order to confirm the existence of compensation, the test of Krug et al. (1976) must be used. This test compares the isokinetic temperature (T_{B}) with the mean harmonic temperature (T_{hm}), which is defined as:

$$T_{\mathrm{hm}} = \frac{n}{\sum_1^n \left(1/T\right)} \quad (11)$$

The confidence interval $(1-\alpha)100$ % for T_{B} could be determined by:

$$T_{\mathrm{B}} = T_{\mathrm{B}} \pm t_{m-2,2\alpha/2}\sqrt{V(T_{\mathrm{B}})} \quad (12)$$

Where:

$$T_{\mathrm{B}} = \frac{\sum\left((\Delta H_{\mathrm{int}})_T - \left(\overline{\Delta H}_{\mathrm{int}}\right)_T\right)\left((\Delta S_{\mathrm{int}})_T - \left(\overline{\Delta S}_{\mathrm{int}}\right)_T\right)}{\sum\left((\Delta S_{\mathrm{int}})_T - \left(\overline{\Delta S}_{\mathrm{int}}\right)_T\right)^2} \quad (13)$$

$$V(T_B) = \frac{\sum\left[(\Delta H_{\mathrm{int}})_T - \Delta G_B - T_B(\Delta S_{\mathrm{int}})_T\right]^2}{(m-2)\sum\left[(\Delta S_{\mathrm{int}})_T - \left(\overline{\Delta S}_{\mathrm{int}}\right)_T\right]^2} \quad (14)$$

According to Krug et al. (1976), a linear chemical compensation pattern exists only if $T_B \neq T_{\mathrm{hm}}$. If T_{hm} falls within the T_B interval, the observed distribution of data in the $(\Delta H_{\mathrm{int}})_T$, $(\Delta S_{\mathrm{int}})_T$ plane is a reflection solely of the propagation of experimental errors, not chemical factors. In this work a 95 % confidence interval for T_B was calculated for all data sets.

Calculation of Moisture Content Corresponding to the Volume of the Micropores

The moisture content corresponding to the volume of the micropores (X_0) was obtained by using the Dubinin–Radushkevich equation (Dubinin et al. 1947):

$$\log\ X = \log\ X_0 - B\log^2\left(\frac{P_v{}^0}{P_v}\right) \tag{15}$$

AFM Images

Firstly, samples were dried out by placing them into a desiccator containing anhydrous phosphorous pentoxide (P_2O_5) during 15 days. A small quantity of capsules was placed onto a small glass surface and subsequently observed through an atomic force microscope (AFM) (MultiMode V brand Vecco, USA). The principle mode of operation of the AFM in the present work was intermittent contact (tapping).

Color Measurement

A colorimeter (Color Flex CX1115 Hunter Lab, USA) was used to measure the apparent color of the samples after 30 days of storage in terms of "L*" (degree of lightness to darkness), "a*" (degree of redness to greenness) and "b*" (degree of yellowness to blueness). The instrument was calibrated with a tile (L*=97.02, a*=0.08, b*=1.75) before the measurements. The samples were placed above the light source in the sample holder of the instrument. Hunter L*, a* and b* values were recorded as the mean of triplicate measurements from three different samples. The hue angle was calculated from the "a*" and "b*" values according to the following equation:

$$\text{Hue angle} = \arctan\left|\frac{b^*}{a^*}\right| \tag{16}$$

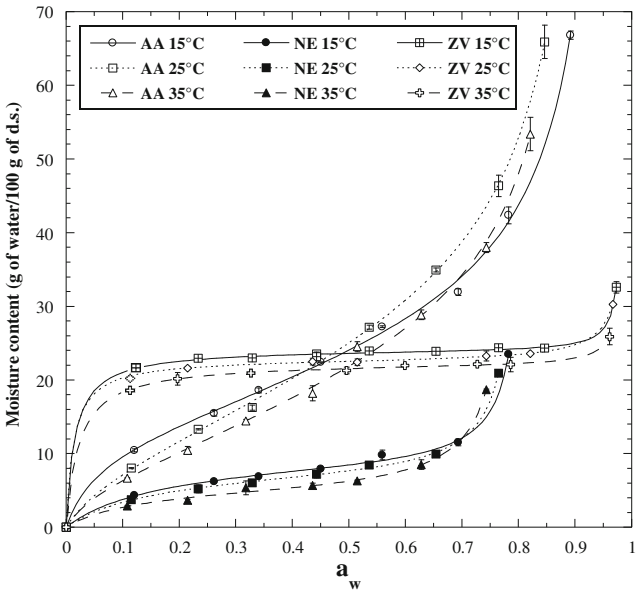

Fig. 1 Moisture adsorption isotherms of AA, NE and ZV. The continuous lines are the fitted points using the DW model

Carotenoids Determination

Carotenoid content was determined through a spectrophotometric method proposed by Hornero and Mínguez (2001). For oleoresin capsules, approximately 0.01 g were dissolved in a volumetric flask containing 25 mL of acetone, then filtered and absorbance measurements were made by using a diode array spectrophotometer (Agilent model 8453) at 472 and 508 nm. Absorbance values were introduced in the following equations to obtain the isochromic carotenoid fractions:

$$C^R = \frac{A_{508}\times 2,144.0 - A_{472}\times 403.3}{270.9} \tag{17}$$

$$C^Y = \frac{A_{472}\times 1,724.3 - A_{508}\times 2,450.1}{270.9} \tag{18}$$

$$C^T = C^R + C^Y \tag{19}$$

All samples were prepared by triplicate and the results were reported with their respective standard deviation in milligram per kilogram of dry capsules.

Modelling and Statistical Analysis

The modelling of the isotherms, the construction of charts and databases were performed with the Kaleida Graph 4.0 Synergy Software package.

Results and Discussion

Figure 1 shows the adsorption isotherms of water vapour at 15, 25 and 35 °C. According to Brunauer et al. (1940), the isotherms of AA and NE can be classified as type II; however, the ZV isotherm is type I. These isotherms are the result of different energetic and structural interactions of the superficial nanostructure of the materials with the water molecules. These interactions can be assessed by the parameters of the DW model, nanoscale features on the surface and the thermodynamic properties of adsorbed water. The ZV isotherm shows a high water adsorption capacity and rapid saturation at low a_w's ($P_v/P_v°$), followed by a second stage in which all the active sites are occupied with water molecules so that a further increment in water activity did not affect water adsorption. This behaviour is also produced because the water molecules

Table 1 Estimated parameters of the D'Arcy–Watt equation for AA, NE and ZV

Material	Parameters	Temperature(°C)		
		15	25	35
(AA)	K'_a	11.137	7.130	4.966
	k_a	17.717	10.116	19.160
	K'_b	4.1092	4.703	4.071
	k_b	1.0137	1.047	1.062
	C	19.605	27.196	25.491
	R	0.999	0.999	0.999
	P (%)	2.106	2.857	2.0377
(NE)	K'_a	9.266	7.888	5.708
	k_a	6.615	7.139	8.032
	K'_b	0.821	0.914	1.001
	k_b	1.214	1.228	1.255
	C	0	0	0
	R	0.997	0.999	0.998
	P (%)	2.033	1.755	3.280
Zeolite Valfor 100 (ZV)	K'_a	24.202	22.875	22.365
	k_a	65.502	76.062	44.995
	K'_b	0.115	0.238	0112
	k_b	1.094	1.003	1.012
	C	0	0	0
	R	0.999	0.999	0.999
	P (%)	0.694	0.252	0.595

are confined in the micropores of ZV. Ng and Mintova (2008) commented that the adsorbents which have type I isotherms are strongly hydrophilic materials due to their high affinity for water at low relative pressures. In respect to AA and NE, they are also hydrophilic materials because they exhibit relatively high adsorption capacities, causing a curve at the beginning of the adsorption isotherm (Fig. 1), but their adsorption capacity is lower than ZV at low water activities. It is interesting to note that, contrary to what one might expect, the isotherm NE is not the result of an additive effect of water adsorption by the alginate and the zeolite, because the adsorption capacity of NE was the lowest of the analysed materials.

The estimated parameters obtained from fitting with the DW model are presented in Table 1. In all cases, maximum water adsorption by strongly binding sites (K'_a) decreased with increasing temperature, a trend which is appropriate since the adsorption is an exothermic process. The opposite effect was observed for water adsorption at secondary sites (indicated by K'_b) for NE material. For AA and ZV materials, an increase in K'_b values from 15 °C to 25 °C was noted but from 25 to 35 °C, these values decreased. K'_b values are related with the formation of a multilayer of water molecules on the primary adsorbed monolayer. AA materials, presented the highest values of K'_b (Table 1), which indicates that this material adsorbed more water molecules at secondary sites of low binding energy than NE and ZV products. Water adsorption by weakly binding sites for the monolayer (C) was considered non-existent for NE and ZV. This agrees with the observations made by D'Arcy and Watt (1970), whose model has the advantage of dispensing with some of its components, so that the calculated parameters have practical significance. The water adsorption at primary (K'_a and C) and secondary (K'_b) sites is the result of two combined mechanisms of water-material interactions, one due to the polar/ionic groups and the other to the three-dimensional space of the structure itself in the material under study. For ZV, the K'_a was about 23 g water/100 g dry solids with high measures of attraction (k_a). In this case, and considering that ZV is a type-A zeolite, the primary adsorption sites correspond to micropores with diameter of 0.4 nm. The structure of A-type zeolite contains large cages having a nearly spherical shape with a diameter of 1.14 nm and a uniform pore size of 0.4 nm (Hui and Chao 2008; Hui et al. 2009). AA capsules have a higher water sorption, which takes place at secondary (K'_b) and weak (C) adsorption sites. In the NE, on the other hand, the strong primary adsorption sites (K'_a) predominate due to the presence of micropores; multilayer adsorption (K'_b) is lower compared with the alginate capsules. These results agree with those published by Azuara and Beristain (2007), who carried out a thermodynamic and kinetic study of water adsorption on whey protein, finding that the amount of water adsorbed at K'_a sites was similar to the water adsorbed in micropores (nanopores with a diameter≤2 nm).

The presence of zeolite in the NE was confirmed by analysing the surface at the nanoscale with atomic force microscopy. In Fig. 2, micropores with pore diameters of 0.4 nm (ultramicropores) can be observed in a zeolite particle embedded in the solid matrix of NE, in contrast to the AA, where the macropores were larger than 90 nm in diameter (Fig. 3). However, this does not mean that the AA does not have any micropores, since it is possible for them to be formed during the gelation of alginate.

Alginate is a linear polysaccharide composed of two monomeric units, β-D-manuronato (M) and α-L-guluronato (G). According to Grant et al. (1973), in the presence of polyvalent ions such as the calcium ion, biopolymer gelation occurs due to strong and specific interactions between ions and blocks of guluronic acid, creating binding sites in the biopolymer chains themselves (Morris et al. 1978). Such binding sites have nanocavities with the ability to retain water molecules, which are important for the formation of the gel (Braccini and Pérez 2001). In this study, we used alginate extracted from *M. pyrifera*, which holds 20 % of the G blocks (Onsøyen 2001). Therefore, in view of the characteristics of the superficial nanostructure ZV, NE and AA, it is possible that K'_a from the DW model represents the adsorption of water in the nanocavities of the order of micropores (Azuara and Beristain 2007; Flores et al. 2007).

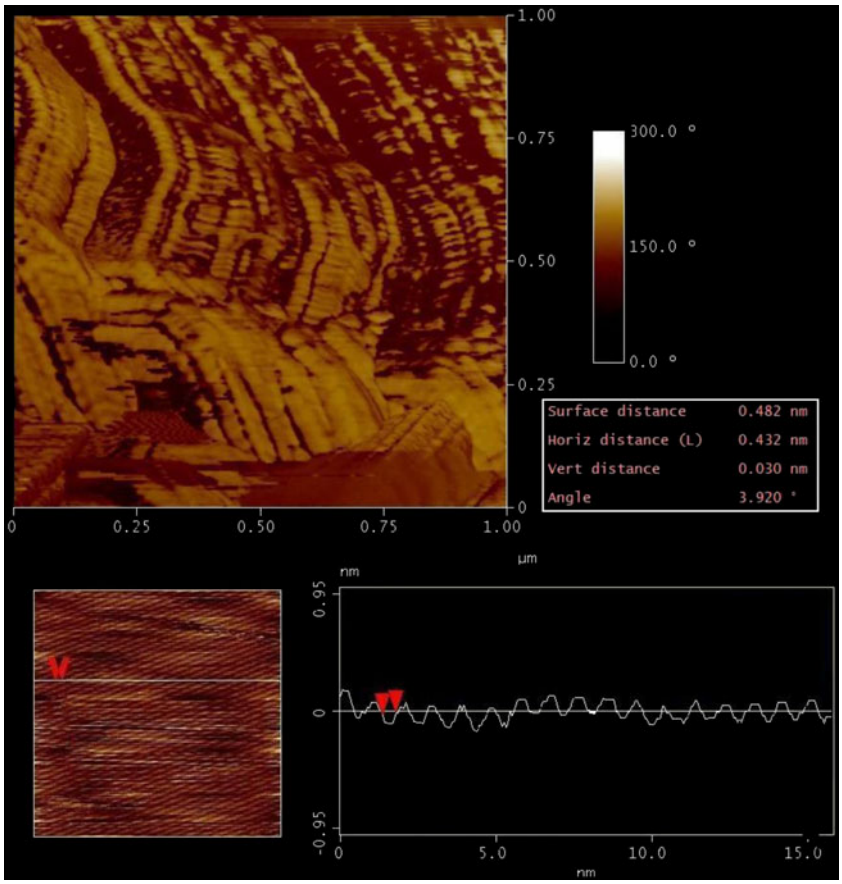

Fig. 2 AFM image of NE surface. Height scale is 0 to 15 nm and profile parallel to *y*-axis. Samples were equilibrated at water activity close to zero

Figure 4 shows the integral entropy of adsorbed water molecules as a function of a_w. The minimum integral entropy is the zone where the water molecules are best organized and less available for taking part in spoilage reactions (Domínguez et al. 2007). For AA, NE and ZV, the minimum ΔS_{int} occurred at 7.0 ($a_w \approx 0.1$), 7.2 ($a_w \approx 0.35$–0.45) and 23.6 ($a_w \approx 0.7$–0.86) g water/100 g dry solids, respectively. These results are within the range of moisture for K'_a, calculated from the DW model (Table 1). In this regard, Azuara and Beristain (2006), found that the adsorbed moisture contents corresponding to the micropore volume, calculated by using the Dubinin–Radushkevich model, matches with the moisture contents at the minimum integral entropy. These authors suggested that increasing the volume of micropores (diameter <2 nm), in food which can be controlled at the nanoscale, could preserve the products with high moisture contents without the water taking part in reactions of deterioration. For AA, NE and ZV materials, the adsorbed moisture content corresponding to the micropore volume (X_0), the moisture content at the minimum integral entropy and the adsorbed moisture content by strongly binding sites (K'_a) are very similar as shown in Table 2. This result is in agreement with findings reported by Azuara and Beristain (2006) and provides evidence that the adsorption process was controlled by entropy when the water molecules were adsorbed in the micropores. Diffusion in micropores is controlled by interactions between the diffusing molecule and the pore walls. Thus, in small pores, steric and other effects associated with the proximity of the pore walls (entropic effects) become important. Besides, the practical use of these results is that by increasing the number of micropores in the solid matrix of wall materials is possible to improve the preservation of nutrients and functional substances during processing and storage.

Figure 5 shows the enthalpy–entropy compensation based on the integral properties of the analysed materials. The zeolite (ZV) showed a straight line of compensation over the entire range of humidity with a $T_{B1}=105.2\pm2.9$ K, $\Delta G_B=-2041$ J/mol. NE capsules showed two straight lines, the first at low moisture contents (0–7.2 g water/100 g dry solids) with a $T_{B1}=164.6\pm2.7$ K, $\Delta G_B=-8533$ J/mol, and the second line, covering the range of remaining moisture with a $T_{B2}=339.7\pm1.7$ K, $\Delta G_B = 306$ J/mol. In the case of AA, it was only possible to estimate a compensation line with a $T_{B2}=387.2\pm3.0$ K, $\Delta G_B=215$ J/mol, since the number of points at low moisture content (<5.8 g water/100 g dry solids) was not enough to estimate a T_{B1}. In all cases, the comparison of T_B's with T_{hm} (297.9 K) confirmed the existence of a thermodynamic compensation. According to the

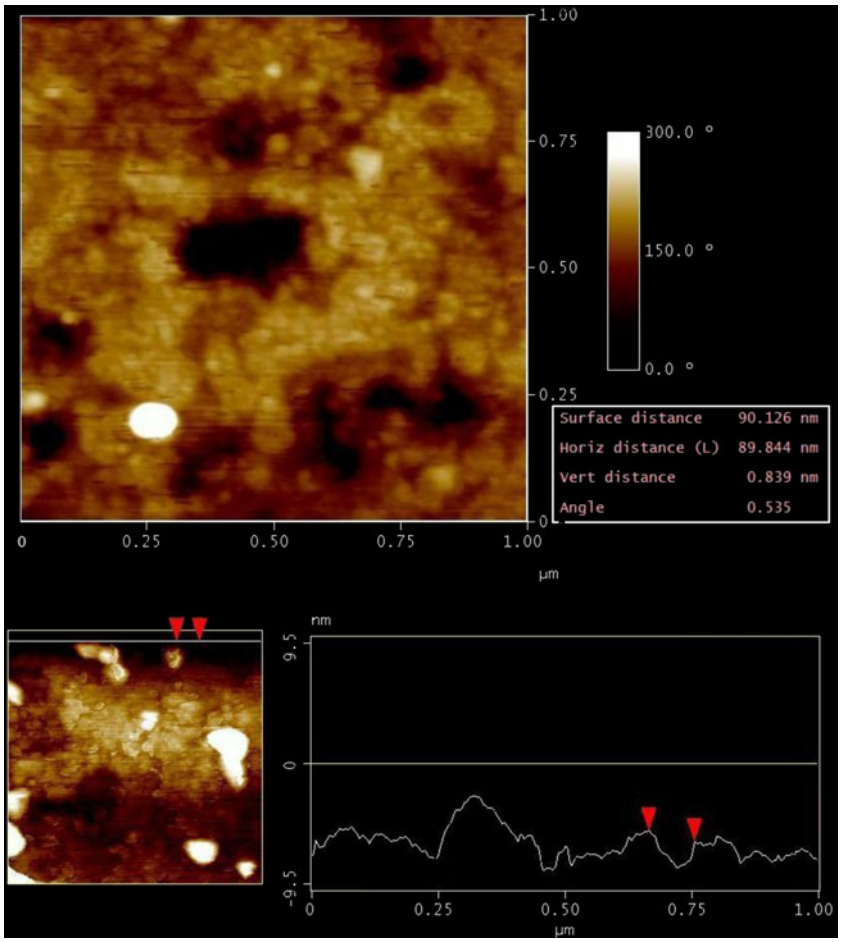

Fig. 3 AFM image of AA surface. Height scale is 0 to 1 µm and profile parallel to *y*-axis. Samples were equilibrated at water activity close to zero

criterion of Leffler (1955), the process is controlled by enthalpy if $T_B > T_{hm}$; on the other hand, if $T_B < T_{hm}$ then the mechanism that controls the process is entropic, like the water adsorption in ZV. The water adsorption for NE at low moisture content is controlled by an entropic mechanism ($T_{B1} < T_{hm}$), i.e., structural aspects such as nanocavities with sizes close to those of the micropores. However, for AA and NE, when the nanocavities (diameter<2 nm) have been saturated with water molecules, then enthalpic control ($T_{B2} > T_{hm}$) begins to dominate. This is due to the affinity of water molecules for the various chemical components (polar or ionic) which form the material. In AA, practically all the adsorption process is controlled by such interactions.

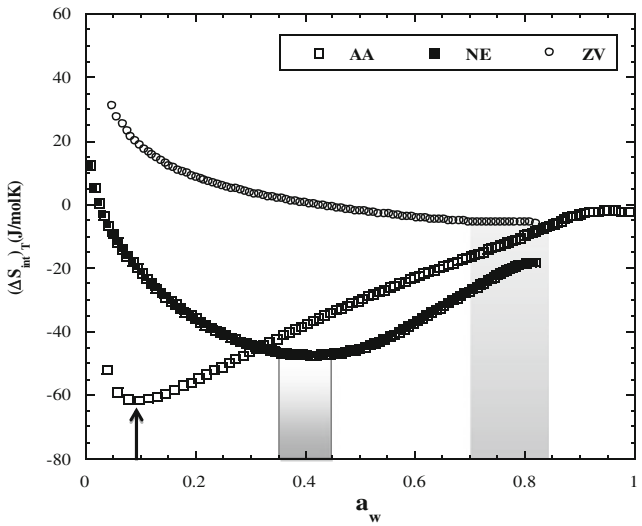

Fig. 4 Integral entropy changes of adsorbed water on AA, NE and ZV as a function of water activity at 25 °C

The enthalpy–entropy compensation has proved a useful tool for the real evaluation of water–food interactions. Flores

Table 2 Moisture content corresponding to the micropore volume (X_0), moisture content at the minimum integral entropy and K'_a parameter for AA, NE and ZV at 25 °C

Material	X_0 (g water/100 g dry solids)	R^2	Moisture at the minimum $(\Delta S_{int})_T$ (g water/100 g dry solids)	K_a' (g water/100 g dry solids)
AA	7.98	0.998	7.0	7.130
NE	8.061	0.983	7.2	7.888
ZV	23.490	0.998	23.6	22.875

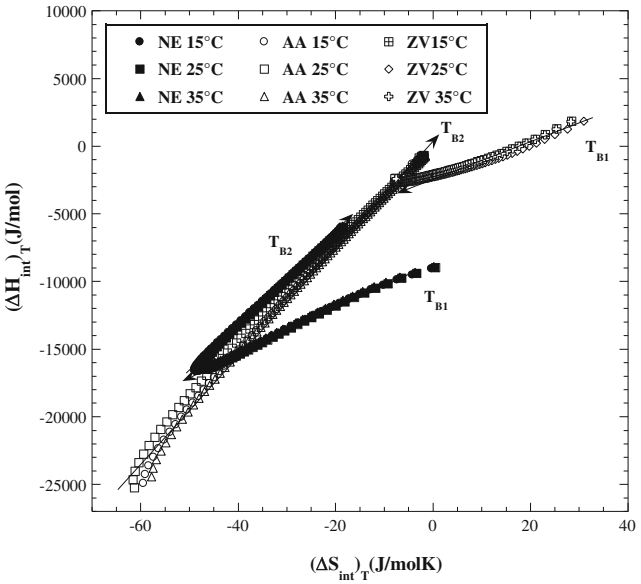

Fig. 5 Enthalpy–entropy relationship for water adsorption in AA, NE and ZV

et al. (2009) demonstrated experimentally with NMR solid state studies that T_B has physical meaning and is appropriate for determining the mechanism that controls the process under study. Their results showed that when the entropic mechanism controls the sorption process, some water molecules are trapped in micropores to the point of minimum molecular mobility. Therefore, it is possible that the same effect is present in the process of water adsorption, so that the molecular mobility of the adsorbed water is reduced as the minimum in ΔS_{int} is obtained, allowing the adsorbed water to act as shielding against spoilage reactions.

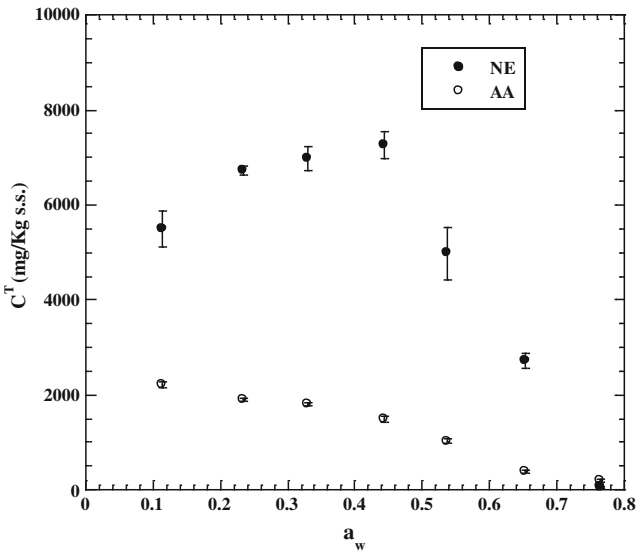

Fig. 6 Carotenoid pigment content as a function of water activity at 25 °C

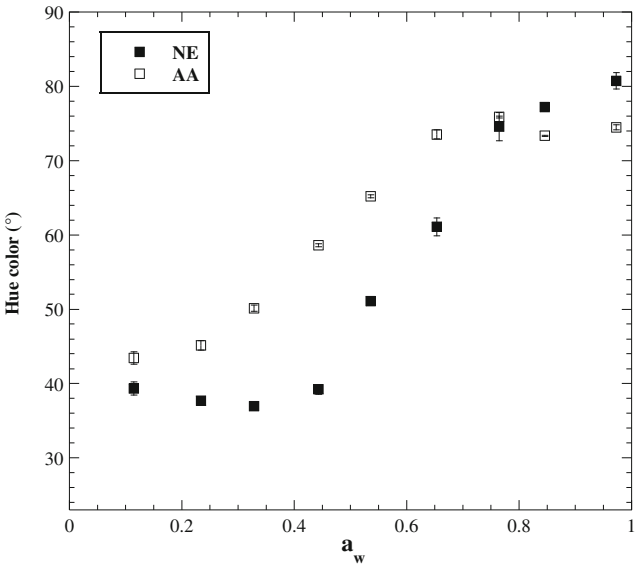

Fig. 7 Hue angle of AA and NE as a function of water activity at 25 °C

The compensation theory has been used recently in nano zinc oxide-loaded calcium alginate film with potential antibacterial properties. These particles were almost homogeneously dispersed within the film matrix, with nearly 60 % particles exhibited an average diameter of 54 nm. In that study,

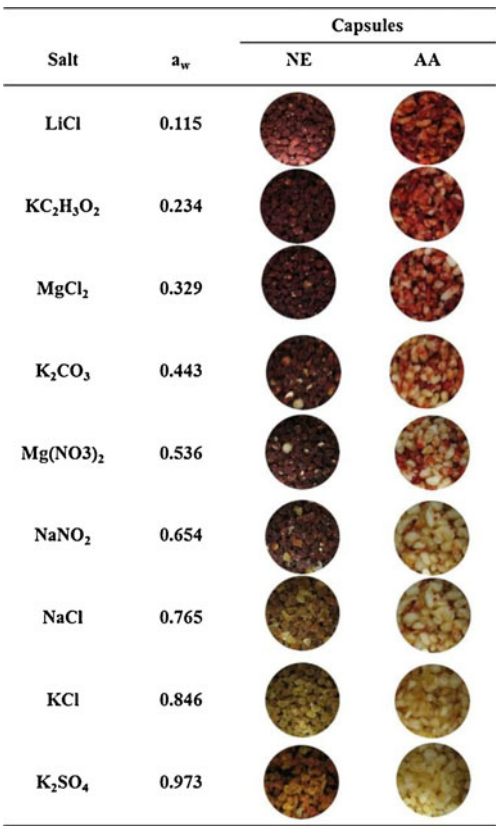

Fig. 8 Gallery of images AA and NE after 30 days of storage as a function of water activity at 25 °C

the moisture uptake mechanism seems to be enthalpy-controlled (Bajpai et al. 2012).

Figures 6 show the carotenoid content as a function of water activity, measured at 30 days of storage. NE capsules contain higher amounts of carotenoids, compared with those of AA. Carotenoids in NE have the typical trend that has been reported for lipids (Labuza et al. 1972; Domínguez et al. 2007; Lavelli et al. 2007). The lower content of carotenoids in 0.1 a_w is due to an autocatalytic oxidation reaction in dehydrated systems (Goldman et al. 1983). When a_w increases, the carotenoid content tends to peak around a range of from 0.35 to 0.45 a_w. These results are consistent with those reported by Lavelli et al. (2007) who found that the minimum degradation of carotenoids in dehydrated carrots occurs at 0.34 to 0.53 a_w.

The zone of minimum integral entropy corresponds to an orderly accommodation of water molecules on and within the nanostructured surface of the product. After this zone of minimum integral entropy, foods tend to be more susceptible to degradation reactions, as is shown by the general trend toward a decrease of carotenoid content in NE just after the ΔS_{int} minimum (Fig. 4) that occurs around 0.35–0.45 a_w. In the case of AA, the contents of carotenoids tend to decrease from 0.1 over almost the entire range of a_w analysed.

Figure 7 represents the hue angle of the capsules of NE and AA measured at 30 days of storage. The hue angle in AA is above 43.48°±0.87 (orange) from 0.1 a_w, whereas the NE hue angle is kept around 39.43°±0.66 (red) to 0.35–0.45 a_w, after which the hue angle tends to increase as water activity increases. Figure 8 shows the visual appearance of the NE and AA capsules with 30 days of storage. Until that time, one can still sense the presence of carotenoids in NE after 0.75 a_w. These results demonstrate that the stability of carotenoids is greater when the food matrix contains a greater micropore volume and the water adsorption mechanism is controlled by entropy in a larger range of water activity.

The thermodynamic analysis of adsorbed water indicates that the entropic mechanism is mainly due to the zeolite nanocavities embedded in the matrix of NE. It is likely that apart from improving the accommodation of water molecules, the nanocavities physically interact with a small part of the structure of carotenoids. An example is β-carotene, with a molecular length of 3 nm, which has been encapsulated in carbon nanotubes from 0.79 to 1.2 nm in diameter (Yanagi et al. 2006). Although the molecular size of carotenoids such as β-carotene is too large to penetrate pores 0.4 nm in diameter, it is possible that the methyl groups and/or cyclic structures of the carotenoids themselves become trapped in these nanocavities, enhancing their stability. Hirano et al. (2000) have reported evidence of such entrapment of organic molecules in zeolite nanopores.

The effect of the entrapment of a small part of the structure of large organic molecules by zeolite helps to explain why the NE has the lowest water-adsorption capacity compared with AA and ZV (Fig. 1). It is likely that the residual monomers of M and G alginate, partially flexible, stay in the zeolite nanocavities, making both materials decrease the number of sites for the adsorption of water and causing the resulting mixture to have less adsorption capacity. It is important to note that the stability of the carotenoids used in this work depends mainly on the entropic mechanism that controls the process and not on its adsorption capacity.

Conclusions

The effect of nanocavities on the adsorption of water could be analysed by the thermodynamic method. The minimum integral entropy made it possible to establish the most appropriate moisture content and a_w for preserving the carotenoids in the materials analysed. Enthalpy–entropy compensation provided important information about the mechanisms for controlling water adsorption. The entropic mechanism was related to the nanoporous structure of the materials analysed, especially with micropores (pore diameter<2 nm); whereas the enthalpic mechanism was related to aspects of chemical affinity for water molecules. The analysis of the carotenoids, and the hue angle, showed that the stability of carotenoids is greater when the water adsorption mechanism is controlled by entropy in a larger range of water activity. These results suggest that by increasing the number and thus the volume of micropores of the material without changing chemical composition of the matrix, it is possible to develop new ingredients, edible films and wall materials with an improved stability during processing and storage of food materials.

References

Azuara, E., & Beristain, C. I. (2006). Enthalpic and entropic mechanisms related to water sorption of yogurt. *Drying Technology, 24*(11), 1–7.

Azuara, E., & Beristain, C. I. (2007). Estudio termodinámico y cinético de la adsorción de agua en proteína de suero de leche. *Revista Mexicana de Ingeniería Química, 6*(3), 359–365.

Babu, V. R., Sairam, M., Hosamani, K. M., & Aminabhavi, T. M. (2007). Preparation of sodium alginate–methylcellulose blend microspheres for controlled release of nifedipine. *Carbohydrate Polymers, 69*(2), 241–250.

Bajpai, S. K., Chand, N., & Chaurasia, V. (2012). Nano zinc oxide-loaded calcium alginate films with potential antibacterial properties. *Food and Bioprocess Technology, 5*(5), 1871–1881.

Beristain, C., & Azuara, E. (1990). Estabilidad máxima en productos deshidratados. *Ciencia, 41*(3), 229–236.

Beristain, C. I., García, H. S., & Azuara, E. (1996). Enthalpy–entropy compensation in food vapor adsorption. *Journal of Food Engineering, 30*(3–4), 405–415.

Braccini, I., & Pérez, S. (2001). Molecular basis of Ca^{2+}-induced gelation in alginates and pectins: the egg-box model revisited. *Biomacromolecules, 2*(4), 1089–1096.

Brunauer, S., Deming, L. S., & Teller, E. (1940). On a theory of van der Waals adsorption of gases. *Journal of the American Chemical Society, 62*(7), 1723–1732.

Chodera, J. D., & Mobley, D. L. (2013). Entropy–enthalpy compensation: role and ramifications in biomolecular ligand recognition and design. *Annual Review of Biophysics, 42*(1), 1–19.

D'Arcy, R. L., & Watt, I. C. (1970). Analysis of sorption isotherms of non-homogeneous sorbents. *Transactions of the Faraday Society, 66*(1), 1236–1245.

Domínguez, I. L., Azuara, E., Vernon-Carter, E. J., & Beristain, C. I. (2007). Thermodynamic analysis of the effect of water activity on the stability of macadamia nut. *Journal of Food Engineering, 81*(3), 566–571.

Dubinin, M. M., Zawierina, E. D., & Raduszkiewicz, L. W. (1947). Sorption and structure of active coals. I. Research on adsorption of organic vapors. *Zurnal Fiziczeskoj Chimii, 21*, 1351–1362.

Flores, E., Pascual, L., Azuara, E., Gutiérrez, G. & Alamilla, L. (2007) Ventajas del modelo de D'Arcy-watt para describir la sorción de vapor de agua en alimentos y otros materiales. In Proceedings of 4º Congreso Internacional de Ingeniería en Movimiento. Puebla, México. March 5–10.

Flores, E., Beristain, C., Vernon-Carter, E., Gutiérrez, G., & Azuara, E. (2009). Enthalpy–entropy compensation and water transfer mechanism in osmotically dehydrated agar gel. *Drying Technology, 27*(9), 999–1009.

Goldman, M., Horev, B., & Saguy, I. (1983). Discoloration of b-carotene in model systems simulating dehydrate foods. Mechanism and kinetic principles. *Journal of Food Science, 48*(4), 751–754.

Grant, G., Morris, E., Rees, D., Smith, P., & Thom, D. (1973). Biological interactions between polysaccharide sand divalent cations: the egg-box model. *FEBS Letters, 32*(1), 195–198.

Hill, P. E., & Rizvi, S. S. H. (1982). Thermodynamic parameters and storage stability of drum dried peanut flakes. *Lebensmittel-Wissenschaft und Technologie, 15*(4), 185–190.

Hirano, T., Li, W., Abrams, L., Krusic, P., Ottaviani, M., & Turro, N. (2000). Supramolecular steric effects as the means of making reactive carbon radicals persistent. quantitative characterization of the external surface of MFI zeolites through a persistent radical probe and a Langmuir adsorption isotherm. *Journal of Organic Chemistry, 65*(5), 1319–1330.

Hornero, M. D., & Mínguez, M. M. I. (2001). Rapid spectrophotometric determination of red and yellow isochromic carotenoid fractions in paprika and re papper oleoresins. *Journal of Agriculture and Food Chemistry, 49*(8), 3584–3588.

Hui, K., & Chao, C. (2008). Methane emissions abatement by multi-ion exchanged zeolite: a prepared from both commercial-grade zeolite and coal fly ash. *Environmental Science & Technology, 42*(20), 7392–7397.

Hui, K., Hui, K., & Seong Kon, L. (2009). A novel and green approach to produce nano-porous materials zeolite a and MCM-41 from coal fly ash and their applications in environmental protection. *World Academy of Science Engineering and Technology, 53*(1), 174–184.

Hummer, G., Rasaiah, J., & Noworyta, J. (2001). Water conduction through the hydrophobic channel of a carbon nanotube. *Nature, 414*(6860), 188–190.

Iiyama, T., Nishikawa, K., Suzuki, T., & Kaneko, K. (1997). Study of the structure of a water molecular assembly in a hydrophobic nanospace at low temperature with in situ X-ray diffraction. *Chemical Physics Letters, 274*(1–3), 152–158.

IUPAC. (1985). Reporting physisorption date. *Pure and Applied Chemistry, 57*, 603.

Johnson, F. A., Craig, D. Q. M., & Mercer, A. D. (1997). Characterization of the block structure and molecular weight of sodium alginates. *Journal of Pharmacy and Pharmacology, 49*(7), 639–643.

Krug, R. R., Hunter, W. G., & Grieger, R. A. (1976). Enthalpy–entropy compensation. 2—Separation of the chemical from the statistical effect. *Journal of Physical Chemistry, 80*(21), 2341–2351.

Labuza, T. P. (1980). Enthalpy/entropy compensation in food reactions. *Food Technology, 34*(2), 67–77.

Labuza, T., McNally, L., Gallagher, D., Hawkes, J., & Hurt, F. (1972). Stability of intermediate moisture foods. Lipid oxidation. *Journal of Food Science, 37*(1), 154–159.

Lang, K. W., McCune, T. D., & Steinberg, M. P. (1981). Proximity equilibration cell for rapid determination of sorption isotherms. *Journal of Food Science, 46*(3), 936–938.

Lavelli, V., Zanoni, B., & Zaniboni, A. (2007). Effect of water activity on carotenoid degradation in dehydrated carrots. *Food Chemistry, 104*(4), 1705–1711.

Leffler, J. E. (1955). The enthalpy–entropy relationship and its implications for organic chemistry. *Journal of Organic Chemistry, 20*(9), 1202–1231.

Lomauro, C. J., Bakshi, A. S., & Labuza, T. P. (1985). Evaluation of food moisture sorption isotherm equations, Part I. Fruit, vegetable and meat products. *Lebensmittel-Wissenchaft and Technology, 18*(2), 111–117.

Martins, S., Sarmento, B., Souto, E. B., & Ferreira, D. C. (2007). Insulin-loaded alginate microspheres for oral delivery—effect of polysaccharide reinforcement on physicochemical properties and release profile. *Carbohydrate Polymers, 69*(4), 725–731.

McMinn, W. A. M., Al-Muhtaseb, A. H., & Magee, T. R. A. (2005). Enthalpy–entropy compensation in sorption phenomena of starch materials. *Food Research International, 38*(5), 505–510.

Morris, E., Rees, D., Thom, D., & Boyd, J. (1978). Chiroptical and stoichiometric evidence of a specific, primary dimerisation process in alginate gelation. *Carbohydrate Research, 66*(1), 145–154.

Ng, E., & Mintova, S. (2008). Nanoporous materials with enhanced hydrophilicity and high water sorption capacity. *Microporous and Mesoporous Materials, 114*(1), 1–26.

Onsøyen, E. (2001). Alginate Production, Composition, Physicochemical Properties, Physiological Effects, Safety, and Food Applications. In S. Sungsoo & M. Dreher (Eds.), *Handbook of dietary fiber*. New York: Taylor & Francis.

Othmer, D. F. (1940). Correlating vapor pressure and latent heat data. A new plot. *Industrial and Engineering Chemistry, 32*(6), 841–856.

Papaioannou, D., Katsoulos, P. D., Panousis, N., & Karatzias, H. (2005). The role of natural and synthetic zeolites as feed additives on the prevention and/or the treatment of certain farm animal diseases: a review. *Microporous and Mesoporous Materials, 84*(1–3), 161–170.

Rizvi, S. S. H., & Benado, A. L. (1984). Thermodynamics properties of dehydrated food. *Food Technology, 38*(3), 83–92.

Rouquerol, F., Rouquerol, J. & Sing, K. (1999) Adsorption by powders and porous solids. Elsevier, pp(20).

Rudra, S. G., Sarkar, B. C., & Shivhare, U. S. (2008). Thermal degradation kinetics of chlorophyll in pureed coriander leaves. *Food Bioprocess Technology, 1*(1), 91–99.

Topuz, A. (2008). A novel approach for color degradation kinetics of paprika as a function of water activity. *LWT- Food Science and Technology, 41*(9), 1672–1677.

Topuz, A., Hao, F., & Mosbah, K. (2009). The effect of drying method and storage on color characteristics of paprika. *LWT- Food Science and Technology, 42*(10), 1667–1673.

Tsami, E., Marinos-Kouris, D., & Maroulis, Z. (1990). Water sorption isotherms of raisins, currants, figs, prunes and apricots. *Journal of Food Science, 55*(6), 1594–1625.

Wexler, A. (1976). Vapor pressure formulation for water in range 0 to 100 °C. A revision. *Journal of Research of the National Bureau of Standards A Physics and Chemistry, 80*(5), 775–785.

Yanagi, K., Miyata, Y., & Kataura, H. (2006). Highly stabilized b-carotene in carbon nanotubes, advanced. *Material, 18*(4), 437–441.